ORIGINAL ARTICLE

Electrically enhanced magnetization in highly strained BiFeO$_3$ films

Jan-Chi Yang[1], Chang-Yang Kuo[1], Heng-Jui Liu[2], Hang-Chen Ding[3], Chun-Gang Duan[3], Hong-Ji Lin[4], Zhiwei Hu[1], Tun-Wen Pi[4], Liu Hao Tjeng[1], Chien-Te Chen[4], Elke Arenholz[5], Qing He[6] and Ying-Hao Chu[2,7]

The control of magnetism via an electric field has attracted substantial attention because of potential applications in magnetoelectronics, spintronics and high-frequency devices. In this study, we demonstrate a new approach to enhance and control the magnetization of multiferroic thin film by an electric stimulus. First, to reduce the strength of the antiferromagnetic superexchange interaction in BiFeO$_3$, we applied strain engineering to stabilize a highly strained phase. Second, the direction of the ferroelectric polarization was controlled by an electric field to enhance the Dzyaloshinskii–Moriya interaction in the highly strained BiFeO$_3$ phase. Because of the magnetoelectric coupling in BiFeO$_3$, a strong correlation between the modulated ferroelectricity and enhanced magnetization was observed. The tunability of this strong correlation by an electric field provides an intriguing route to control ferromagnetism in a single-phase multiferroic.

INTRODUCTION

To implement multifunctional, low-power consumption and 'green' nanoelectronics, electrical control of the spin degree of freedom is an intriguing route to explore. Promising approaches, as well as a new field of physics, focus on using magnetoelectric multiferroics,[1,2] in which an electric field can be used to switch or alter the inherent magnetic order.[3–9] Furthermore, applications based on multiferroics, such as logic, memory and high-frequency devices, have been developed over the past decade,[10,11] providing new varieties of next-generation electronic devices.

To achieve electric control of magnetism in multiferroics, various material systems have been proposed and studied experimentally.[1,12,13] Single-phase magnetoelectric multiferroics—materials that show spontaneous magnetization and polarization simultaneously—are favored, but they remain elusive under ambient conditions. Two alternate pathways to obtain multiferroicity have been widely adopted. One method is to start with intrinsic magnetic materials, such as manganites, and to strategically develop improper ferroelectricity therein.[14,15] Another method is to add magnetic ions to a traditional ferroelectric material, such as BaTiO$_3$, to induce a magnetic moment.[16–18] Although both approaches have been demonstrated conceptually, they share common challenges: (1) the order temperature of the developed materials is in most cases too low for practical applications; (2) the induced magnetization/ferroelectricity cannot be arbitrarily modulated by external electric/magnetic fields, because of weak coupling between the magnetization and ferroelectricity. One unique exception is BiFeO$_3$ (BFO), which exhibits a strong coupling between ferroelectricity and antiferromagnetism at room temperature (ferroelectric $T_C \sim 830\,°C$, antiferromagnetic $T_N \sim 370\,°C$).[19] Weak ferromagnetism has been detected in BFO thin films;[20,21] therefore, enhancing the magnetization of BFO is the most intuitive way to remove obstacles to the practical application of electric field control of magnetism.

In this study, we demonstrate a controllable means of enhancing the magnetization in highly strained BFO thin films. This goal was accomplished via use of (1) a highly distorted BFO phase to reduce the antiferromagnetic superexchange interaction, which manifests itself in a reduced antiferromagnetic Néel temperature, as determined by X-ray linear dichroism (XLD) and (2) an electric field-driven rotation of the ferroelectric polarization to enhance the Dzyaloshinskii–Moriya (DM) interaction, as supported by density-functional theory (DFT) calculations. The enhanced moment was detected by X-ray magnetic circular dichroism (XMCD), and the strong magnetoelectric coupling was revealed by photoemission electron microscopy (PEEM). Our results provide a promising route to engineer BFO thin films for next-generation nano-electronics.

[1]Max-Planck Institute for Chemical Physics of Solids, Dresden, Germany; [2]Department of Materials Science and Engineering, National Chiao Tung University, Hsinchu, Taiwan, ROC; [3]Key Laboratory of Polar Materials and Devices, Ministry of Education, East China Normal University, Shanghai, China; [4]National Synchrotron Radiation Research Center, Hsinchu, Taiwan, ROC; [5]Advanced Light Source, Lawrence Berkeley National Laboratory, Berkeley, CA, USA; [6]Department of Physics, Durham University, Durham, UK and [7]Institute of Physics, Academia Sinica, Taipei, Taiwan, ROC
Correspondence: Professor Q He, Department of Physics, Durham University, Room 235, Rochester Building, Science Site, South Road, Durham DH1 3LE, UK.
E-mail: qing.he@durham.ac.uk
or Professor Y-H Chu, Department of Materials Science and Engineering, National Chiao Tung University, Room 709, Engineering Building VI, 1001 University Road, Hsinchu 30010, Taiwan, ROC.
E-mail: yhc@nctu.edu.tw
Received 15 June 2015; revised 5 February 2016; accepted 1 March 2016

MATERIALS AND METHODS
Thin film growth and structure characterization
Thirty nanometer BFO films were deposited by pulsed laser deposition at 700 °C in 100 mTorr of oxygen. The growth was monitored by high-pressure reflective high-energy electron diffraction. The films were subsequently cooled in 1 atm of oxygen to room temperature. For electrical poling experiments, a thin $LaNiO_3$ (~ few unit cells) layer was inserted as a bottom electrode deposited under the same growth conditions as for the BFO. X-ray diffraction (XRD) was used to confirm the crystallinity and to determine the strain state of the BFO films.

Magnetic characterization and analysis
The magnetic properties of the BFO films were investigated using polarization-dependent soft X-ray absorption spectroscopy (XAS). The experiments were conducted at beamlines 11A and 08B at the National Synchrotron Radiation Research Center (NSRRC) in Taiwan. The energy resolution at the Fe-$L_{2,3}$ edges ($h\nu$ = 700–730 eV) was set to 0.25 eV, and the degree of linear polarization of the incident X-ray beam was 99%. The spectra were collected in total-electron-yield mode, and a single Fe_2O_3 crystal was measured simultaneously in a separate chamber to calibrate the photon energy with an accuracy better than 10 meV. The antiferromagnetic and ferromagnetic domain structure in the BFO films was further studied using PEEM at beamline 11.0.1 at the Advanced Light Source, Lawrence Berkeley National Laboratory.

RESULTS AND DISCUSSION
To enhance the magnetization of BFO strategically, as a first step, we used strain engineering by depositing BFO on pseudo-cubic (pc) $(001)_{pc}$ single-crystal substrates with different lattice parameters, including $LaAlO_3$ (LAO, a = 3.79 Å), $NdGaO_3$ (NGO, a = 3.86 Å), $SrTiO_3$ (STO, a = 3.90 Å) and $DyScO_3$ (DSO, a = 3.94 Å). Figure 1a shows the out-of-plane (OOP) XRD θ-2θ scans of BFO films grown on these substrates. Only $(00L)_{pc}$ peaks of BFO and peaks contributed by the substrates were observed, indicating that the growth direction of BFO thin films is along the c-axis regardless of substrate. The c-axis lattice parameters of BFO films extracted from the XRD results were 3.98, 4.04, 4.17 and 4.64 Å for the films grown on DSO, STO, NGO and LAO, respectively, thus indicating that the BFO films are subjected to different epitaxial strains due to the lattice mismatch between the substrate and the film. To further investigate the structure of highly strained BFO films on NGO substrates, we used grazing incidence XRD to record the in-plane (IP) reciprocal space maps. Figure 1b shows the reciprocal space maps around the $(110)_{pc}$ diffraction feature of NGO, in which the reciprocal space units were normalized to the lattice constant of the NGO substrate ($a_{pc} \approx 3.86$ Å). The BFO $(110)_{pc}$ peak was detected at (0.995 1.0), corresponding to a and b lattice

constants of 3.87 Å and 3.86 Å. Furthermore, the c/a ratio of the BFO films on NGO reached 1.083, thus confirming that the film exhibits a large biaxial compressive strain imposed by the substrate. The distorted structure of BFO on NGO is similar to the previously observed highly distorted rhombohedral phase in the mixed-phase BFO system (a mixture of rhombohedra-like and tetragonal-like phases).[22] This highly distorted rhombohedral phase shows an enhanced spontaneous magnetization in the mixed-phase system.[23] Therefore, enhanced ferromagnetism can be expected in highly distorted BFO films on NGO.

To investigate the ferroelectric domain structure of the highly strained BFO films, piezo-response force microscopy (PFM) was used. Domains with upward and downward polarizations give rise to opposite contrasts (dark and bright, respectively) in the OOP-PFM images, whereas the IP components of polarization can produce a torque on the cantilever of the microscope, resulting in contrast in the IP-PFM images. By combining the OOP-PFM and IP-PFM images, we were able to identify the polarization direction of each domain. The PFM results are summarized in Figure 2. The center square corresponds to a region after electrical poling, whereas the as-grown (un-poled) region is located outside the square. A uniform bright contrast in the OOP channel indicates a single downward ferroelectric component along the OOP direction. The IP-PFM image shows a stripe-like pattern with three levels of contrast—dark (black), neutral (brown) and bright (white). Dark and bright contrasts correspond to the IP polarization components pointing along the $[1-10]_{pc}$ and $[-110]_{pc}$ directions, whereas the neutral contrast corresponds to the IP polarization components pointing along either $[-1-10]_{pc}$ or $[110]_{pc}$. These results indicate that the domain structure of the BFO films on NGO is characterized by four polarization variants.

To investigate the ferroelectric switching behavior in the highly distorted BFO films, the response of the ferroelectric polarization to an applied DC bias via a conducting AFM tip was studied. Figures 2a–c show the IP-PFM of the same area with the central square switched by an applied bias of −4, −6 and −9 V, respectively. The domain structure in the switched area changed as a function of the applied poling voltage. With −4 V applied through the tip, the domain structure of the poled area (Figure 2a) showed a near perfect alignment of stripe-like domains with a contrast level similar to the as-grown area. When the poling voltage was increased to −6 V, a lower IP-PFM contrast in the poled area compared with the as-grown area was observed. With the tip scanning along the $[1-10]$ axis in this image, each scan line crossed both the poled and as-grown areas, thus precluding degradation of the tip as a reason for changes in contrast
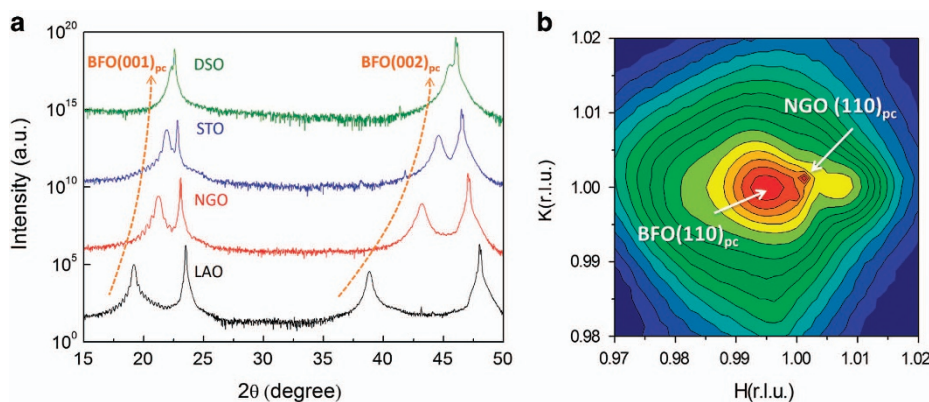

Figure 1 Structure analysis of highly strained $BiFeO_3$ (BFO) thin film. (**a**) θ-2θ scans for 30-nm BFO films as a function of the epitaxial strain imposed by various substrates. (**b**) In-plane reciprocal space mapping of the highly distorted BFO phase on an $NdGaO_3$ (NGO) substrate.
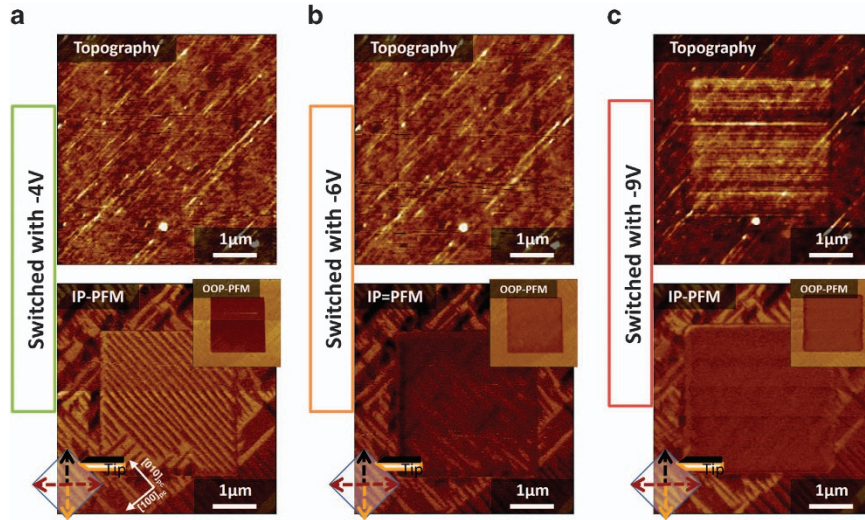
Figure 2 Responses of the ferroelectric domains to an external electric field. The topography and piezo-response force microscopy (PFM) images of the same area with a central square poled by (**a**) − 4 V, (**b**) − 6 V and (**c**) − 9 V. The insets show the out-of-plane (OOP)-PFM contrasts for the same area.
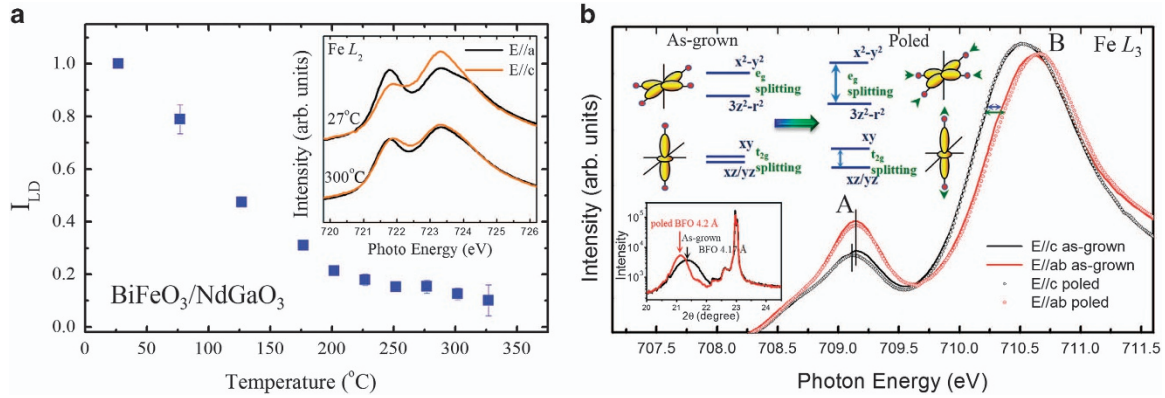

Figure 3 X-ray absorption spectroscopy studies of highly strained $BiFeO_3$ (BFO) thin films. (**a**) The temperature-dependent I_{LD} for BFO/NdGaO$_3$ (NGO), where the inset figure shows the soft X-ray absorption (XA) spectra measured at 27 and 300 °C at the Fe L_3 edge with the X-ray linear polarization E parallel to *c* (E//*c*, orange line) and perpendicular to *c* (E⊥*c*, black line). (**b**) The XA spectra with E//*c* and E⊥*c* for the as-grown (solid curves) and poled (dotted curves) BFO/NGO thin films. The inset shows the corresponding change in the *c*-axis observed via X-ray diffraction (XRD). The orbital nature and structure variation are illustrated in the schematics of the inset.

levels. The 'fading' domain structure of the poled area indicated that the ferroelectric polarization lost its IP components during the electrical poling process. As the poling voltage further increased to − 9 V, no detectable IP component was found in the poled area, thus suggesting that the ferroelectric polarization of the poled area is rotated predominantly to the OOP direction. This result indicates that a meta-stable state is created after − 9 V poling, and a ferroelectric polarization aligned along the $[001]_{pc}$ direction was observed in the distorted BFO crystal structure constrained by the NGO substrate. Remarkably, this process is reversible because of the ferroelectric nature of BFO, as summarized in the Supplementary Materials (Supplementary Figure S1a and b). These results clearly demonstrate that the ferroelectric polarization in the highly distorted BFO phase can be tailored by an external electric field. Now, a key question arises: how is this intriguing feature coupled to the antiferromagnetism as well as to the inherent ferromagnetism of BFO?

The polarization dependence of XAS is determined by magnetic contributions[24,25] and crystal field effects,[25,26] which, in the present case, are directly related to the antiferromagnetism and ferroelectricity

of BFO.[19] The magnetic contribution to the XLD can be determined by monitoring the linear dichroism as a function of temperature: the magnetic XLD is expected to decrease rapidly when the sample is heated to the Néel temperature (T_N).[25,27] A reduction of the XLD with increasing temperature is shown in the inset of Figure 3a for the highly strained BFO films. Temperature-dependent I_{LD} at the Fe-L_2 edge is shown in Figure 3a, where I_{LD} is the integration of the absolute XLD signal, that is, $|\text{E}//\text{a-E}//\text{c}|^2$ from 721 eV to 726 eV (see the inset) normalized to the value measured at room temperature. Compared with that of bulk BFO, a much lower T_N of ∼ 230 °C was observed. The Néel temperature of BFO is dominated by the strength of the exchange interaction (J), which can be expressed by:

$$J \approx |t|^4 / (U^* \, \Delta^2)$$

where *t* represents the overlap integral between the oxygen 2*p* orbital and the Fe *d* orbital in a one-electron Hamiltonian, whereas *U* and Δ stand for the on-site Coulomb repulsion and charge transfer energy, respectively.[27,28] For d^5 systems, the primary interaction is between the two filled e_g orbitals via the oxygen 2*p* σ-bonding orbitals. The
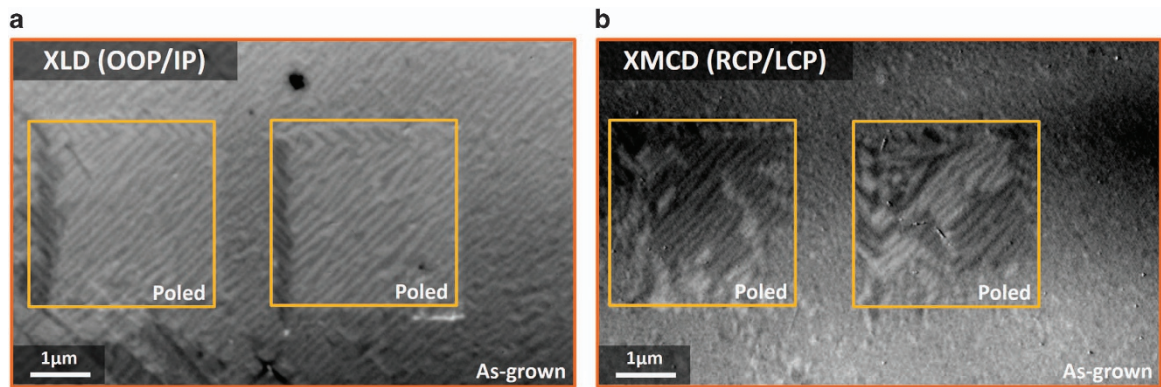
4

Figure 4 Photoemission electron microscopy imaging of the electrical control of magnetism in highly strained BiFeO$_3$ (BFO) thin films. (**a**) X-ray linear dichroism (XLD)-photoemission electron microscopy (PEEM) and (**b**) X-ray magnetic circular dichroism (XMCD)-PEEM images for the poled (yellow-squared areas) and un-poled (as-grown) regions in a highly strained BFO thin film.

increased Fe-O distance along the c-direction as well as the deviation of the Fe-O-Fe bond angle from 180º within the ab plane, as compared with bulk BFO, would give rise to a decrease in the hopping integral, resulting in a suppression of the antiferromagnetic Néel temperature. Therefore, the reduced T_N suggests a reduction of the superexchange interaction in our highly strained BFO films, which in turn is expected to enhance the canted moment of BFO because the magnitude of the moment strongly depends on the competition of the superexchange and DM interactions.

In addition to understanding the influence of strain engineering on the antiferromagnetic order of highly strained BFO, it is crucial to study the effect of the electrical poling. Before the XAS measurement, the polarization of the poled samples was switched by a scanning probe technique with a 2-axis motor setup (scanning voltage set to − 9 V) to obtain an upward polarized area of ∼ 4 mm^2, which is much larger than the X-ray beam size (several hundred μm^2). The Fe-L_3 XAS spectra taken with **E** parallel to the c-axis (in black) and parallel to the a-axis (in red) are shown in Figure 3b for both the as-grown (solid lines) and poled (dots) films. The energy shifts at peaks A and B of the spectra taken with **E**//**c** and **E**//**a** can be attributed to the splitting of the t_{2g} and e_g orbitals, respectively. The energy of the electron transition from the 2p core level to the $d(x^2 − y^2)$ states was higher than that to the $d(3z^2 − r^2)$ states, resulting in a larger energy difference between peak A and peak B of **E**//**c** compared with that of **E**//**a**. More importantly, we observed an increase of the splitting in the e_g (40 meV) and t_{2g} (20 meV) orbitals for the poled BFO film. Such an increase implies a larger c/a ratio of the film after the electrical poling process. The corresponding energy diagrams and configurations are illustrated in the inset of Figure 3b. Good agreement was found with the XRD measurements (shown in the inset of Figure 3b) for both samples: we found a measurable increase in the lattice parameter along the c-axis and a narrower full width at half maximum for the poled sample. Such a result excludes sample damage as a result of the poling process and as the origin of the change in c/a. Additionally, a perceptible change of surface topography (Figure 2c) also supports the above conclusion. These results indicate that the structure of the highly strained BFO is elongated along the c-direction after the electrical poling procedure. Our results strongly support the unique feature of ferroelectric polarization between the two phases, a distorted rhombohedral BFO with the polarization along $<111>_{pc}$ and an extremely compressive strained phase with the polarization along $<001>_{pc}$,[29] thus suggesting an potentially promising means of modulating the intermediate phases between the rhombohedral and

tetragonal BFO phases. This finding should lead to electrically controllable magnetization in BFO.

The correlation of antiferromagnetic and ferromagnetic orders in the highly strained BFO films was further studied using PEEM. Figures 4a and b show the XLD- and XMCD-PEEM images of a highly strained BFO film, with yellow squares indicating areas where the ferroelectric polarization has been switched by an applied voltage of − 9 V to point toward the sample surface (upward). The XLD-PEEM images show the ratio between images taken at the two most prominent features of the Fe^{3+} L_2 edge with linearly polarized X-rays (**E** vector in the sample surface) at a grazing X-ray incidence angle ($\theta = 30°$). A clear stripe-like domain structure in the poled and un-poled areas can be observed in the XLD-PEEM image, where the switched regions can be easily identified by the discontinuity of domains and the change of domain alignment. The polarization of the poled region is now in a ferroelectric mono-domain state according to the PFM result (Figure 2c). Therefore, the stripe-like domain structure observed in the poled region in the XLD-PEEM image can be attributed mainly to the antiferromagnetic domains.

To reveal the ferromagnetic component in the highly strained BFO film, XMCD-PEEM images were obtained using both left circularly polarized and right circularly polarized X-rays in a grazing incidence geometry ($\theta = 30°$). To enhance the magnetic contrast and eliminate contributions from the topography, the ratio of the two images is shown. The image contrast is effectively a map of the local IP magnetization vector; that is, regions with magnetic moments aligned parallel to the X-ray wave vector appear bright, whereas those that are antiparallel appear dark. No ferromagnetic contrast was detectable above the noise level in the as-grown area. The poled area in this image shows regular stripe-like ferromagnetic domains. Moreover, the XLD- and XMCD- PEEM images in the poled region show a one-to-one correlation. The highly correlated nature of the anti-ferromagnetic and ferromagnetic domain structures in the switched area suggests that the enhanced magnetization can be attributed to a canted Fe moment in the otherwise antiferromagnetically ordered BFO. This result demonstrates an electric field-driven magnetization in the highly strained BFO film. Such enhanced magnetism can further be used to enhance the exchange coupling with a ferromagnetic layer adjacent to a BFO layer because the canted magnetic moment in BFO has a key role in controlling the magnetization in the ferromagnet/BFO heterostructures.[30,31]

To provide more insight into the experimental findings, we conducted DFT calculations using the projector augmented-wave
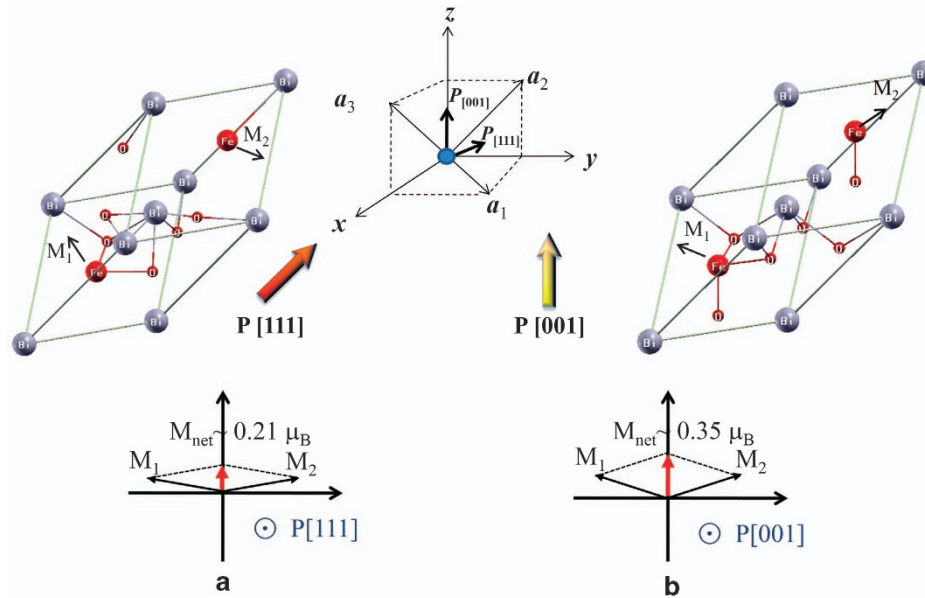
Figure 5 Schematic illustration of the electric field-induced magnetization change (**a**) The as-grown state of a BiFeO$_3$ (BFO) film on NdGaO$_3$ (NGO), in which the polarization points along the [111]$_{pc}$ direction. The canting angle of the as-grown strained BFO thin film attributed to the Dzyaloshinskii–Moriya (DM) interaction is approximately 3°, whereas the net magnetization is ~0.21 μ_B; (**b**) the poled state, in which the polarization rotates toward the [001]$_{pc}$ direction. The canting angle of the poled BFO is ~5°, whereas the resultant magnetization is 0.35 μ_B.

method as implemented in the Vienna *ab initio* simulation package.[32] The Perdew–Burke–Ernzerhof form of the generalized gradient approximation for exchange and correlation was used.[33] The cutoff energy was 500 eV, and a $4 \times 4 \times 4$ k-point sampling was used in a self-consistent calculation. The effective Hubbard constant ($U_{eff} = U - J = 2.0$ eV) for the Fe $3d$ electrons was chosen to give a better description of the strongly correlated systems.[34] To simulate the polarization switching of BFO on NGO substrates, we used a pseudo-cubic monoclinic BFO structure with an IP lattice constant of 3.86 Å and G-type antiferromagnetic order,[29,35] as shown in Figure 5. The OOP unit cell parameter was varied to minimize the total energy, and all internal coordinates were relaxed until the Hellmann-Feynman forces on the relaxed atoms were less than 2 meV Å^{-1}. The ferroelectric polarization direction of the ground state of BFO in such a structure is close to but not exactly along [111]$_{pc}$, in agreement with the experiment. To determine the [001]$_{pc}$ polarization state, we started from a paraelectric pseudo-cubic structure with fixed Bi ions and then moved the Fe ions gradually along the pseudo-cubic [001]$_{pc}$ direction until the total energy was minimized. During the search for the stable state with [001]$_{pc}$ polarization, the O ions were allowed to be fully relaxed.

The DM interaction arises from the spin-orbit coupling in the superexchange,[36] which involves non-collinear magnetism. Following Ederer and Spaldin,[20,37] we performed two sets of non-collinear magnetic structure calculations, that is, one for the nearly [111]$_{pc}$ polarized state and the other for the [001]$_{pc}$ polarization. The canting angle of unstrained BFO was calculated to be 1°, which results in a small magnetization of 0.05 μ_B.[20] Furthermore, we found that for the highly strained BFO with a nearly [111]$_{pc}$ as-grown polarized state, the canting angle is approximately 3° and increases to 5° for the [001]$_{pc}$ polarized state. Our calculations indicate that the magnetic moments of individual Fe ions in the two polarization states are similar, that is, 3.96 and 3.94 μ_B for the nearly [111]$_{pc}$ and [001]$_{pc}$ polarized states, respectively. In addition, the rotation angles of the oxygen octahedra around the c-axis with respect to the [111] and [001] polarizations

were deduced to be 8.9° and 11°, respectively. Consequently, the magnetization caused by the DM interaction in BFO increases from 0.21 to 0.35 μ_B per formula unit when the ferroelectric polarization is switched from the [111]$_{pc}$ direction to the [001]$_{pc}$ direction (see Figure 5), qualitatively agreeing with the experiments. Further proof for a stronger DM interaction is the increase of the magnetocrystalline anisotropy energy when the nearly [111]$_{pc}$ polarized state switches to the [001]$_{pc}$ state. The magnetocrystalline anisotropy energis are 0.12 and 0.88 meV per formula unit for the nearly [111]$_{pc}$ and [001]$_{pc}$ states, respectively, suggesting a significant increase of the spin-orbit coupling, which then amplifies the DM interactions. However, the DFT calculation simulates a relatively ideal supercell at $T = 0$ K; thus, the calculated values can only be qualitatively interpreted.

CONCLUSION

We applied strain engineering and electric fields to significantly enhance the inherent magnetization of BFO. The decreased T_N due to large compressive strain was characterized using XLD, indicating the reduction of the superexchange interaction. PFM studies combined with DFT calculations demonstrated the feasibility of enhancing the DM interaction in the highly strained BFO phase via an electrical modulation of the ferroelectric polarization. XMCD and PEEM measurements demonstrated the electrically controllable nature of the enhanced magnetizations and the strong correlation between the enhanced magnetization and multiferroicity in BFO films. Our study adds a new scenario to the electric field control of magnetism and sheds light on next-generation and low-power spintronics.

1 Spaldin, N. A. & Fiebig, M. The renaissance of magnetoelectric multiferroics. *Science* **309**, 391–392 (2005).

2 Eerenstein, W., Mathur, N. D. & Scott, J. F. Multiferroic and magnetoelectric materials. *Nature* **442**, 759–765 (2006).

3 Lebeugle, D., Colson, D., Forget, A., Viret, M., Bataille, A. M. & Gukasov, A. Electric-field-induced spin flop in BiFeO3 single crystals at room temperature. *Phys. Rev. Lett.* **100**, 227602 (2008).

4 Lee, S., Ratcliff, W., Cheong, S. W. & Kiryukhin, V. Electric field control of the magnetic state in $BiFeO_3$ single crystals. *Appl. Phys. Lett.* **92**, 192906 (2008).

5 Lottermoser, T., Lonkai, T., Amann, U., Hohlwein, D., Ihringer, J. & Fiebig, M. Magnetic phase control by an electric field. *Nature* **430**, 541–544 (2004).

6 Ramesh, R. & Spaldin, N. A. Multiferroics: progress and prospects in thin films. *Nat. Mater.* **6**, 21–29 (2007).

7 Cheong, S. W. & Mostovoy, M. Multiferroics: a magnetic twist for ferroelectricity. *Nat. Mater.* **6**, 13–20 (2007).

8 Scott, J. F. Room-temperature multiferroic magnetoelectrics. *NPG Asia Mater.* **5**, e72 (2013).

9 Fusil, S., Garcia, V., Barthelemy, A. & Bibes, M. Magnetoelectric devices for spintronics. *Annu. Rev. Mater. Res.* **44**, 91–116 (2014).

10 Bibes, M. & Barthélémy, A. Multiferroics: towards a magnetoelectric memory. *Nat. Mater.* **7**, 425–426 (2008).

11 Ma, J., Hu, J., Li, Z. & Nan, C. W. Recent progress in multiferroic magnetoelectric composites: from bulk to thin films. *Adv. Mater.* **23**, 1062 (2011).

12 Heron, J. T., Trassin, M., Ashraf, K., Gajek, M., He, Q., Yang, S. Y, Nikonov, D. E., Chu, Y. H., Salahuddin, S. & Ramesh, R. Electric-field-induced magnetization reversal in a ferromagnetic-multiferroic heterostructure. *Phys. Rev. Lett.* **107**, 217202 (2011).

13 Martin, L. W., Chu, Y. H. & Ramesh, R. Advances in the growth and characterization of magnetic, ferroelectric, and multiferroic oxide thin films. *Mater. Sci. Eng. R Rep.* **68**, 89–134 (2010).

14 Kimura, T., Goto, T., Shintani, H., Ishizaka, K., Arima, T. & Tokura, Y. Magnetic control of ferroelectric polarization. *Nature* **426**, 55–58 (2003).

15 Aken, B. B. V., Palstra, T. T. M., Filippetti, A. & Spaldin, N. A. The origin of ferroelectricity in magnetoelectric YMnO3. *Nat. Mater.* **3**, 164–170 (2004).

16 Lin, Y. H., Yuan, J., Zhang, S., Zhang, Y., Liu, J., Wang, Y. & Nan, C. W. Multiferroic behavior observed in highly orientated Mn-doped BaTiO3 thin films. *Appl. Phys. Lett.* **95**, 033105 (2009).

17 Ramana, E. V., Yang, S. M., Jung, R., Jung, M. H., Lee, B. W. & Jung, C. U. Ferroelectric and magnetic properties of Fe-doped BaTiO3 thin films grown by the pulsed laser deposition. *J. Appl. Phys.* **113**, 187219 (2013).

18 Apostolova, I. N., Apostolov, A. T., Bahoosh, S. G., Bahoosh, S., J. M. & Wesselinowa. Origin of ferromagnetism in transition metal doped BaTiO3. *J. Appl. Phys.* **113**, 203904 (2013).

19 Zhao, T., Scholl, A., Zavaliche, F., Lee, K., Barry, M., Doran, A., Cruz, M. P., Chu, Y. H., Ederer, C., Spaldin, N. A., Das, R. R., Kim, D. M., Baek, S. H., Eom, C. B. & Ramesh, R. Electrical control of antiferromagnetic domains in multiferroic BiFeO3 films at room temperature. *Nat. Mater.* **5**, 823–829 (2007).

20 Ederer, C. & Spaldin, N. A. Weak ferromagnetism and magnetoelectric coupling in bismuth ferrite. *Phys. Rev. B* **71**, 060401(R) (2005).

21 Martin, L. W., Chu, Y. H., Holcomb, M. B., Huijben, M., Yu, P., Han, S. J, Lee, D, Wang, S. X. & Ramesh, R. Nanoscale control of exchange bias with BiFeO3 thin films. *Nano Lett.* **8**, 2050–2055 (2008).

22 Damodaran, A. R., Liang, C. W., He, Q., Peng, C. Y., Chang, L., Chu, Y. H. & Martin, L. W. Nanoscale structure and mechanism for enhanced electromechanical response of highly strained BiFeO3 thin films. *Adv. Mater.* **23**, 3170–3175 (2011).

23 He, Q., Chu, Y. H., Heron, J. T., Yang, S. Y., Liang, W. I., Kuo, C. Y, Lin, H. J., Yu, P., Liang, C. W., Zeches, R. J., Kuo, W. C., Juang, J. Y., Chen, C. T., Arenholz, E., Scholl, A. & Ramesh, R. Electrically controllable spontaneous magnetism in nanoscale mixed phase multiferroics. *Nat. Commun.* **2**, 225 (2011).

24 Nolting, F., Scholl, A., Stohr, J., Seo, J. W., Fompeyrine, J., Siegwart, H., Locquet, J. P., Anders, S., Luning, J., Fullerton, E. E., Toney, M. F., Scheinfein, M. R. & Padmore, H. A. Direct observation of the alignment of ferromagnetic spins by antiferromagnetic spins. *Nature* **405**, 767–769 (2000).

25 Csiszar, S. I., Haverkort, M. W., Hu, Z., Tanaka, A., Hsieh, H. H., Lin, H. J, Chen, C. T., Hibma, T. & Tjeng, L. H. Controlling orbital moment and spin orientation in CoO layers by strain. *Phys. Rev. Lett.* **95**, 187205 (2005).

26 Hollmann, N., Hu, Z., Willers, T., Bohatý, L., Becker, P., Tanaka, A., Hsieh, H. H., Lin, H.-J., Chen, C. T. & Tjeng L. H. Local symmetry and magnetic anisotropy in multiferroic MnWO4 and antiferromagnetic CoWO4 studied by soft X-ray absorption spectroscopy. *Phys. Rev. B* **82**, 184429 (2010).

27 Ko, K. T., Jung, M. H., He, Q., Lee, J. H., Woo, C. S., Chu, K., Seidel, J., Jeon, B. G., Oh, Y. S., Kim, K. H., Liang, W. I., Chen, H. J., Chu, Y. H., Jeong, Y. H., Ramesh, R., Park, J. H. & Yang, C. H. Concurrent transition of ferroelectric and magnetic ordering around room temperature. *Nat. Commun.* **2**, 567 (2011).

28 Maekawa, S., Tohyama, T., Barnes, S. E., Ishihara, S., Koshibae, W. & Khaliullin, G. in *Physics of Transition Metal Oxides*. (Springer, Berlin, Heidelberg, Germany, 2004).

29 Zeches, R. J., Rossell, M. D., Zhang, J. X., Hatt, A. J., He, Q., Yang, C. H, Kumar, A., Wang, C. H., Melville, A., Adamo, C., Sheng, G., Chu, Y. H., Ihlefeld, J. F., Erni, R., Ederer, C., Gopalan, V., Chen, L. Q., Schlom, D. G., Spaldin, N. A., Martin, L. W. & Ramesh, R. A strain-driven morphotropic phase boundary in BiFeO3. *Science* **326**, 977–980 (2009).

30 Chu, Y. H., Martin, L. W., Holcomb, M. B., Gajek, M., Han, S. J., He, Q., Balke, N., Yang, C. H., Lee, D., Hu, W., Zhan, Q., Yang, P. L., Fraile-Rodríguez, A., Scholl, A., Wang, S. X. & Ramesh, R. Electrical-field control of local ferromagnetism using a magnetoelectric multiferroic. *Nat. Mater.* **7**, 478–482 (2008).

31 Heron, J. T, Bosse, J. L., He, Q., Gao, Y., Trassin, M., Ye, L., Clarkson, J. D., Wang, C., Liu, J., Salahuddin, S., Ralph, D. C., Schlom, D. G., Iñiguez, J., Huey, B. D. & Ramesh, R. Deterministic switching of ferromagnetism at room temperature using an electric field. *Nature* **516**, 370–373 (2014).

32 Kresse, G. & Furthmuller, J. Efficiency of ab-initio total energy calculations for metals and semiconductors using a plane-wave basis set. *Comput. Mater. Sci.* **6**, 15–50 (1996).

33 Perdew, J. P., Burke, K. & Ernzerhof, M. Generalized gradient approximation made simple. *Phys. Rev. Lett.* **77**, 3865–3868 (1996).

34 Dudarev, S. L., Botton, G. A., Savrasov, S. Y., Humphreys, C. J. & Sutton, A. P. Electron-energy-loss spectra and the structural stability of nickel oxide: An LSDA +U study. *Phys. Rev. B* **57**, 1505–1509 (1998).

35 Hatt, A. J. & Spaldin, N. A. Strain-induced isosymmetric phase transition in BiFeO3. *Phys. Rev. B* **81**, 054109–054113 (2010).

36 Moriya, T. Anisotropic superexchange interaction and weak ferromagnetism. *Phys. Rev.* **120**, 91–98 (1960).

37 Ederer, C. & Spaldin, N. A. Electric-field-switchable magnets: the case of $BaNiF_4$. *Phys. Rev. B* **74**, 020401–020404 (2006).

Supplementary Information accompanies the paper on the NPG Asia Materials website (http://www.nature.com/am)